Article

Engineering the Quaternary Hydrotalcite Derived Ce-Promote Ni-Based Catalysts for Enhanced Low-Temperature CO_2 Hydrogenation into Methane

Yu xin Peng , Xin Xiao * , Lei Song , Ning Wang , Wei Chu *

Posted Date: 23 May 2023

doi: 10.20944/preprints202305.1552.v1

Keywords: Ce dopants; Ni-based catalyst; CO2 methanation; lower temperature performance; Quaternary hydrotalcites

Article

Engineering the Quaternary Hydrotalcite Derived Ce-Promote Ni-Based Catalysts for Enhanced Low-Temperature CO_2 Hydrogenation into Methane

Yuxin Peng [1], Xin Xiao [2,3,*], Lei song [1], Ning Wang [4] and Wei Chu [1,*]

[1] School of Chemical Engineering, Sichuan University, Chengdu, 610065, China
[2] College of Carbon Neutrality Future Technology, Sichuan University, Chengdu, 610106, China
[3] National Engineering Research Centre for Flue Gas Desulfurization, Chengdu, 610065, China
[4] College of Environmental and Energy Engineering, Beijing University of Technology, Beijing 100124, China
* Correspondence: xiaoxin93@scu.edu.cn (X.X.); chuwei1965@scu.edu.cn (W.C.)

Highlights:

- Ce-promoted NiCex-C catalysts were derived from the Ce-containing quaternary hydrotalcite through the co-precipitation method.
- Ce dopants regulated the interaction between Ni and Mg(Ce)AlOx, modifying the basic species and increasing the surface $Ni^0/(Ni^{2+}+ Ni^0)$ ratio.
- The threefold TOF was correlated to the tailored surface medium-strength basic sites and achieved over the NiCe5-C sample with 80% conversion of CO_2 at 250 °C.

Abstract: Ce-promoted NiMgAl mixed-oxide (NiCex-C, x = 0, 1,5,10) catalysts were prepared from the quaternary hydrotalcite precursors for CO_2 hydrogenation to methane. By engineering the Ce contents, NiCe5-C showed its prior catalytic performance in low-temperature CO_2 hydrogenation, being about 3 times higher than that of Ce-free NiCe0-C catalyst (TOF of NiCe5-C and NiCe0-C: 1.19 h^{-1} vs 0.39 h^{-1} @ 250 °C). With extensive characterization, it was found that Ce dopants promoted the reduction of NiO by adjusting the interaction between Ni and Mg(Ce)AlOx support. The higest ratio of surface $Ni^0/(Ni^{2+}+Ni^0)$ was obtained over NiCe5-C. Meanwhile, the surface basicity was tailored with Ce dopants. The strongest medium-strength basicity and highest capacity of CO_2 adsorption was achieved on NiCe5-C with 5wt% Ce content. The TOF tests indicated a good correlation with medium-strength basicity over the NiCex-C samples. The results showed that the high medium-strength and Ce-promoted surface Ni^0 species endows the enhanced low-temperature catalytic performance in CO_2 hydrogenation to methane.

Keywords: Ce dopants; Ni-based catalyst; CO_2 methanation; lower temperature performance; Quaternary hydrotalcites

1. Introduction

Recently, CO_2 reduction and recycling has become one of the most research topics in neutral carbon economics due to the serious impact on global climate change led by the growing CO_2 emissions[1,2].To migrate the increasing authropogenic CO_2, methods like CO_2 capture, utilization and storage (CCUS)had been engaged [3]. Among these methods, the conversion of CO_2 with "green hydrogen" (hydrogen originates from sustainable energy, like wind, solar. Etc.) into synthetic natural gas (SNG) has been considered as one of the most promising and practical approaches for CO_2 utilization[4,5]. SNG, as a high value-added fuel product, plays a vital role as a raw material in the synthesis of syngas and many chemical products[6]. CO_2 hydrogenation to SNG reaction, which was also called Sabatier reaction, displayed a great potential in "Power to Gas" process[7]. However, this reaction went through an eight-electron process for CO_2 reduction into methane, which suffered an significant kinetic limitations [8]. To solve this puzzle, a catalytic material could achieve high reaction rates was required. Ni-based catalysts with high reaction activity and low-cost, aroused extensive

 doi:10.20944/preprints202305.1552.v1

interest of researchers[9]. While, in practical application, Ni-based catalysts always suffered from inferior activity at low temperatures[10]. Compared to CO_2 methanation reaction in a higher-temperature, the low-temperature CO_2 methanation showed advantages in two different aspects: (I) The competitive reaction like reverse water gas shift (RWGS) reaction could be effectively reduced at low temperatures, and the catalysts obtained a high CH_4 selectivity. (II) The sintering and carbon deposition problems of the catalyst usually occurred at high temperatures, low temperature condition was conducive to the catalysts stability[11–13]. Therefore, improving the low temperature activity of Ni-based catalysts is a current research hotspot[14].

Hydrotalcite (HT) was a kind of natural or synthetic ordered materials, which consisted of positively charged two-dimensional sheets of mixed hydroxides, and charge-compensating anions placed between the layers[15]. They were expressed as $[M^{2+}_{1-x}M^{3+}_x(OH)_2]\ (A^{n-})_{x/n} \cdot mH_2O$. ($M^{2+}$ and M^{3+} were divalent and trivalent metals, respectively; x was the mole ratio of $M^{3+}/(M^{2+}+M^{3+})$, A^{n-} was the interlayer anion)[7].The unique supramolecular structure provided great potential to disperse and tune active sites at the atomic scale[16]. Introduce a proportion of alkaline elements into the HT precursor could obtain a tunable alkaline site structure and promote the CO_2 adsorption, which would benefit for the CO_2-involving reaction. For instance, the addition of Mg element could improve the catalyst basic properties, result in the increase of the CO_2 adsorption capacity[17]. Moreover, small-size and heat-stable metal nanoparticles were highly dispersed on the calcined HT precursor surface after reduction, thus the catalyst stability and reducibility would get enhanced [10]. For example, Guo et al. synthesized the hydrotalcite-derived NiMgAl catalyst exhibited the excellent catalytic activity with CO_2 conversion of 91.8% at 250°C[18]. Therefore, it was a promising approach by fabricating the alkaline-assisted hydrotalcite-derived materials to obtain the efficient low-temperature catalyst for CO_2 methanation.

However, traditional NiMgAl catalyst derived from hydrotalcite also suffered from strong metal-support interaction[19], thus a long-time H_2 reduction process was needed to enhance reducibility. To overcome this drawback, quite a few reports were found to introduce a second metal (such as Mn, La and Y) to replace partial Mg element [20,21], thereby regulating the metal-support interaction. As reported by our group, the doping of Mn element could efficiently regulated the Ni and Mg(Mn)AlOx interaction, surface content of Ni^0 species, and basic property[11]. Dominik Wierzbicki et al. supposed La could soften the interaction between Ni and the HT matrix, lead to the increase of Ni-species reducibility [22]. Sun et al. found the incorporation the 0.4 wt% Y strongly decreased the metallic nickel particle size and increased the medium-strength basic sites[23].

Besides the Mn, La,Y species, Ce, as a rare earth oxide, had also been a very attractive promoter for the CO_2 methanation due to its extraordinary ability to enhance metal dispersion as well as the thermal stability of the support [24,25]. Dębek R et al. found CeO_2 had a promoting effect on increasing surface basicity of the catalyst, which was attributed to the its high mobile oxygen capacity and redox activity [26]. Reducing CO_2 to CO process was the rate-determining step of CO_2 methanation. In addition, the oxygen vacancy provided by the CeO_2 could create an additional driving force for this process in the reducing atmosphere [27]. Zhang et al. considered that Ce^{3+} cations located in the $AlCeO_3$ solid solution could greatly promote the adsorption and activation of CO_2 and facilitate the formation of the intermediate, therefore the CO_2 conversion was significantly accelerated at low reaction temperatures[28]. In dry reforming of methane (DRM) reaction, Radosław Debek et al. incorporated Ce-species into the NiMgAl catalysts, which was found to promote the nickel species reducibility and introduce new strong oxygen species (low coordinated) and more medium-strength basic sites (Lewis acid-base pairs) [15,29].

Furthermore, a recent literature compared different Ni content (10.3, 16.2, 27.3, 36.8, 42.5 wt.%) on the performance of hydrotalcite-derived catalysts, the optimum Ni content was 42.5wt%. This result confirmed the higher amount of Ni introduced led to smaller crystallites, better reducibility and CO_2 adsorption capacity of the catalysts. H_2-TPR proved the Ni and hydrotalcite matrix interaction weakened with the increasing Ni contents, which had a positive effect on the catalytic activity[30]. However, according to our knowledge, quaternary hydrotalcite-derived Ce-containing Ni-Ce catalysts had not been widely used in CO_2 methanation. Herein, our goal was to study the

structure-performance relationships between them. We prepared a series of Ce-promoted Ni/MgAlOx catalysts through co-precipitation method in this study. The low-temperature catalytic performance was investigated by varying Ce content from 0, 1, 5 to 10wt%. The optimal sample displayed superior CO_2 methanation activity with 80% CO_2 conversion at low temperature 250°C, and the CH_4 selectivity was close to 100%. Meanwhile the CO_2 conversion (91.7%) was not deactivated upon 80h operation at 300°C. Extensive characterization methods (XRD, BET, ICP SEM, TEM, XPS, H_2-TPR, CO_2-TPD) were used to deeply analyze the promoting effect of Ce on influencing the catalyst structure, morphology, surface properties, metal-support interaction, performances during CO_2 methanation.

2. Experimental

2.1. Catalyst Synthesis

All of the hydrotalcite precursors were prepared by the co-precipitation method. Ni content was kept at 40wt % and the Mg/Al molar ratio was fixed at 1 in all samples, while the loading of Ce varied from 0, 1, 5 to 10wt%. Firstly, the mixture of $Ni(NO_3)_2{\cdot}6H_2O$, $Mg(NO_3)_2{\cdot}6H_2O$, $Al(NO_3)_3{\cdot}9H_2O$, $Ce(NO_3)_3{\cdot}6H_2O$ was dissolved in the deionized water to form a solution at 0.4 M. Then the mixed nitrate solution was added dropwise into a flask containing 280mL sodium carbonate solution (0.25M) at 60°C under vigorous stirring. At the same time, keeping the slurry PH at 9.5-10 by adding the sodium hydroxide solution (1M). After co-precipitation, the slurry was vigorous stirred at 60°C for 1h and then aged for 18 h at 60°C. The solid product was obtained by filtration, washed with deionized water for three times, dried at 60°C overnight, and named as NiCe0-HT (without Ce), NiCex-HT (x=1,5,10). Finally, the obtained hydrotalcite precursors were calcined at 500°C for 4 h, and labeled as NiCex-C (x=0,1,5,10).

2.2. Catalytic Experiments

CO_2 methanation reaction was performed in a miniature fixed-bed reactor at atmospheric pressure. 200 mg catalyst (40-60 mesh) mixed with 500 mg quartz sand were placed in the quartz tube (inner diameter of 6mm and a length of 40cm). Prior to the catalyst evaluation, the catalysts were reduced under 30ml/min H_2 at 700 °C for 2 h. After reduction, the catalyst bed was cooled down in the N_2 atmosphere to 180 °C, then the mixture of 40ml/min H_2 and 10ml/min CO_2 (H_2: CO_2=4:1, GHSV=15000 ml/ g/ h) was introduced into the reactor. The catalytic test was carried out in the temperature range of 200-350 °C at a temperature interval of 25°C. The gas products were analyzed by an on-line SP-7890 gas chromatogram equipped with a thermal conductivity detector (TCD) (fitted with a TDX01 column). Taking the CO_2 conversion (X_{CO2}) and the CH_4 selectivity (S_{CH4}) as indicators to evaluate the activity of the catalysts, which were calculated by the following equations[31]:

$$X_{CO_2} = \left(\frac{F_{CO_2,in} - F_{CO_2,out}}{F_{CO_2,in}}\right) \times 100\% \quad (1)$$

$$S_{CH_4} = \left(\frac{F_{CH_4,out}}{F_{CO_2,in} - F_{CO_2,out}}\right) \times 100\% \quad (2)$$

where "$F_{CO2,\ in}$" and "$F_{CO2,\ out}$" refer to the inlet CO_2 gas flow and the outlet CO_2 gas flow respectively, "$F_{CH4,\ out}$" refer to the outlet CH_4 gas flow, mL/min.

The equations of CO_2 conversion rate (R_{CO2}, μmolCO_2/(g_{cat}·s)) and Turnover frequency (TOF, h^{-1}) are as follows[32,33].

$$R_{CO_2} = \frac{F_{CO_2,in} \times X_{CO_2}}{m \times V_m} \quad (3)$$

where V_m represents the gas molar volume of 22.4 L/mol under standard conditions, X_{CO2} refers to the conversion of CO_2 at 225 °C (X_{CO2}<15%), m denotes the quality of the catalyst (g)[11,34]

Preprints (www.preprints.org) | NOT PEER-REVIEWED | Posted: 23 May 2023 doi:10.20944/preprints202305.1552.v1

$$\mathrm{TOF} = \frac{F_{\mathrm{CO_2,in}} \times \delta}{N_{surface} \times \mathrm{V_m}} \quad (4)$$

$$\mathrm{N_{surface}} = \mathrm{N_{total}} \times \mathrm{D} \quad (5)$$

where δ represents the methane yield and $\mathrm{N_{surface}}$ represents the molar amount of nickel atoms located on the catalyst surface, which is calculated by the nickel dispersion equation (D, %) based on the size of Ni nanoparticles after reduction (TEM reault).

The apparent activation energy of the catalyst was measured according to Arrhenius equation:

$$\ln k = lnk_0 - \frac{E_a}{RT} \quad (6)$$

where k is the reaction rate, k_0 is the pre-exponential factor, Ea is the apparent activation energy of the reaction, R is the gas reaction constant (8.314 J/(mol·K)), and T is the reaction temperature. The experimental conditions were carefully selected to obtain the catalytic data with CO_2 conversion below 15% for activation energy calculation, which effectively excluded the influence of diffusion limit[34].

2.3. Characterization of Catalysts

Powder X-ray diffraction (XRD) measurement was performed on Rigaku Ultma IV device equipped with a copper-based anode (Cu Kα radiation, λ=0.154 nm). The instrument settings were 35 kV× 30 mA. It operated in the 2θ range from 5° to 85° with the scanning speed of 2°·min $^{-1}$, to identify the crystal phase and morphology of the sample.

The hydrogen temperature-programmed reduction (H_2-TPR) measurement was performed on a TP-5080 instrument equipped with a TCD detector (Tian jing, Xian quan) to investigate the reduction performance of the catalyst. Firstly, 50mg catalyst was placed in the quartz tube, then 30ml/min N_2 was put into the instrument for 1 h at 200 ℃ to remove the physical adsorbed impurities on the catalyst surface. After cooling down to 50 ℃ under argon, 28ml/min 10% H_2/N_2 mixture was introduced to reduce the catalyst, and the system was kept at 50 ℃ for 40min until the baseline was stable. Then the reactor temperature was linearly increased from 50℃ to 800℃ at a heating rate of 5℃/min.

The carbon dioxide temperature-programmed desorption (CO_2-TPD) was carried out on a Auto Chem II 2920 apparatus to determine the basic sites on catalyst surface. Firstly, 0.1g catalyst was placed in the quartz tube, 30ml/min H_2/Ar was put into the device for 10 min at room temperature to remove the residual gas in the tube. Then the catalyst was reduced in H_2/Ar at 700℃ for 2 h. After that, the sample was cooled down to 50℃ in N_2 atmosphere. After CO_2 adsorption of the catalyst for 1h, N_2 was put into to the system to remove the remained CO_2 in the gas phase and the physically adsorbed CO_2 on the catalyst surface. Finally, the system was heated from 50℃ to 800℃ at a linear heating rate of 10℃/min to desorb the chemisorbed CO_2 on the catalyst surface.

The N_2 adsorption-desorption analysis was carried out on the ASAP 2020 analyzer at -196℃. All samples were degassed at 300℃ for 6 h before the analysis to desorb contaminants and moisture. The specific surface area was characterized by adsorption isotherm according to the multiple Brunauere-Emmette-Teller (BET) equation. The pore size distribution and average pore diameter were determined by the Barrette-Joynere-Halenda (BJH) model. Inductively coupled plasma optical emission spectrometer (ICP-OES) was carried out by an Agilent 5110(OES) equipment to conduct elemental analysis of the catalysts.

X-ray photoelectron spectroscopy (XPS) measurements were performed over a Thermo Scientific K-Alpha spectrometer equipped with Monochromated Al Kα X-ray source, (hυ =1486.6 eV, 12 kV, 6 mA). The binding energy standard was C1s=284.80eV.

ZEISS Sigma 30 scanning electron microscope (SEM) was used to study the morphology of the catalyst precursor. The acceleration voltage was 3 kV and the magnification was 5W and 10W times. Moreover the morphology, metal dispersion and lattice spacing of the calcined and reduced catalysts

Preprints (www.preprints.org) | NOT PEER-REVIEWED | Posted: 23 May 2023 doi:10.20944/preprints202305.1552.v1

were characterized by field emission transmission electron microscopy (TEM), which was performed on FEI Tecnai G2 F20 instrument with an acceleration voltage of 200 kV.

3. Results and Discussion

3.1. Texture Characteristics of the NiCex-C Catalysts

Figure 1a showed the XRD diffraction profiles of precursors with various Ce contents. Distinct diffraction peaks were observed at 2θ~11°, ~22°, ~34°, ~38°, ~46°, ~60°, ~61° for all the samples, which belonging to (003), (006), (012), (015), (018), (110), and (113) of hydrotalcite characteristic structure (JCPDS-22-0700)[11]. In particular, compared with Ce-free sample, obviously weaker and wider diffraction peaks were observed in other Ce-containing samples. This results indicated that the Ce doping could influence the crystallinity of the sample, and disturb the hydrotalcite plate layer structure[35]. **Figure 1b** showed XRD spectrum of samples after calcination at 500℃ for 4 h, it could be found that the hydrotalcite structure was destroyed and obtained the mixed metal oxide. The peaks at 2θ=37.3°, 43.3°, 62.9°, 75.5° were corresponded to (111), (200), (220) and (311) crystal planes of NiO, respectively (JCPDS-47-1049)[36]. After adding Ce element, the intensity of these characteristic peaks in the samples decreased significantly. Meanwhile, well-crystallized CeO_2 could be observed after calcination. And the peaks at 28.5°, 33.0°, 47.4°, and 56.3° were indexed to (111), (200), (220) and (311) crystal planes of CeO_2 (JCPDS-34–0394)[37]. In special, the diffraction peaks corresponding to MgO and Al_2O_3 were absent. The Al and Mg species may form as a amorphous structure or being a part of the $MgAl_2O_4$ spinel, whose diffraction peaks were overlapped by the periclase[11,38].

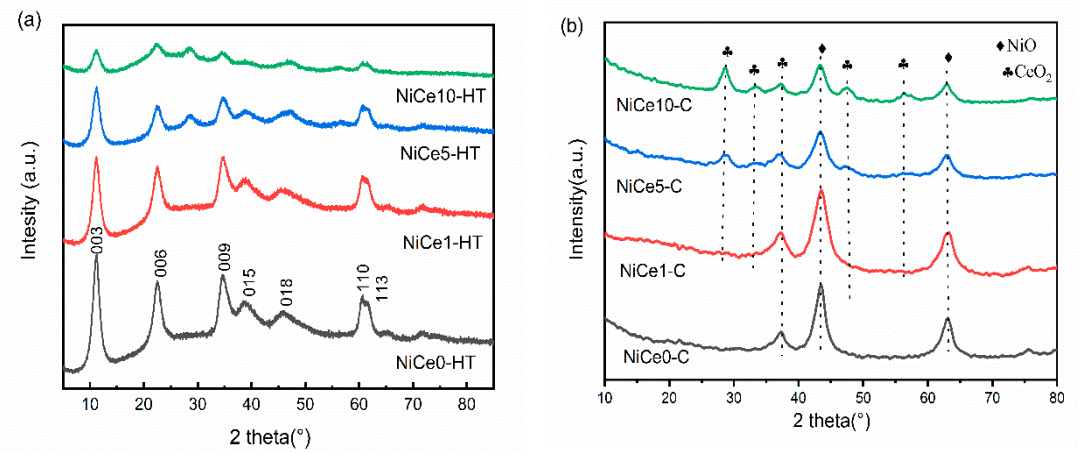

(**a**) (**b**)

Figure 1. XRD patterns of the hydrotalcite-like precursors NiCex-HT (**a**) and the mixed oxides NiCex-C (**b**).

Texture properties of the NiCex-C catalysts were investigated by N_2 adsorption-desorption analysis. As presented in **Figure 2a**, according to the IUPAC classification, all the samples displayed an IV N_2 adsorption-desorption isotherm (P/P_0>0.4) with H2 hysteresis loops, corresponding to the typical feature of mesoporous structure[3]. The pore structure might be caused by the stack of 2D structure of HT, which was conducive to the adsorption and activation of active gases, promoting the mass transmission process[39]. As shown in **Figure 2b**, all samples featured typical mesoporous structures with narrow pore size distributions, concentrated on 2 to 10 nm. In addition, the detailed textural properties of the NiCex-C catalysts were listed in **Table 1.** All the catalysts derived from hydrotalcite-like compounds displayed large specific surface area (>100 m^2/g), which allowed for a better dispersion of surface nickel species[40]. The mean pore diameters of the catalysts were all slightly decreased after the introduction of Ce element. It mainly due to the Ce species on the external porous surface of the hydrotalcite crystallites, causing the blockage of partial smaller mesoporous

Preprints (www.preprints.org) | NOT PEER-REVIEWED | Posted: 23 May 2023 doi:10.20944/preprints202305.1552.v1

[41]. On the other hand, there was no significant difference on the average pore volume among all samples.

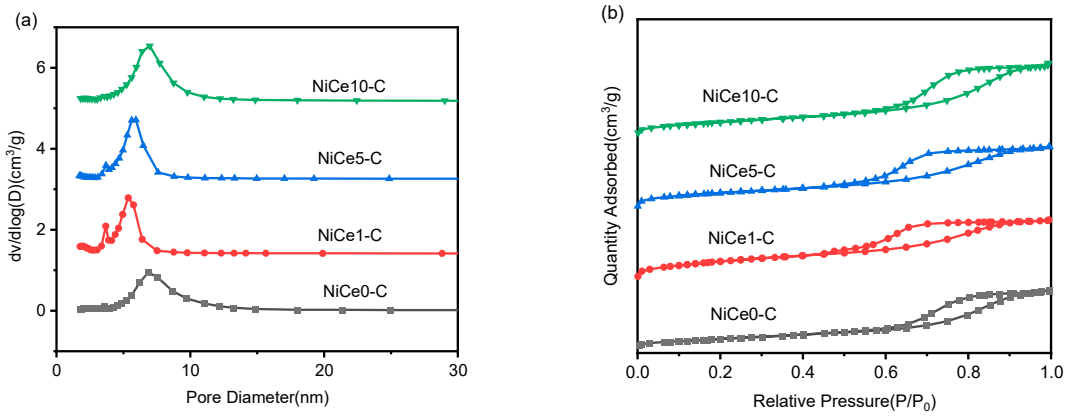

Figure 2. N_2 adsorption-desorption isotherms (**a**) and distributions of pore size of the NiCex-C catalysts.

Table 1. Detail information of textural properties of the NiCex-C catalysts.

Sample	S_{BET}[a](m^2/g)	V_p[b](cm^3/g)	D_p[c](nm)	Ni[d]%	Ce[e]%	Mg/Al[f]
NiCe0-C	127.7	0.24	6.41	44.5	0.0	1.5
NiCe1-C	215.0	0.25	6.25	40.5	0.79	1.5
NiCe5-C	176.9	0.26	5.24	40.1	4.07	1.5
NiCe10-C	169.0	0.29	4.37	42.3	8.70	1.4

a BET specific surface area. b Calculated from the adsorption amount of N_2 at a relative pressure (P/P0) of 0.98. c BJH Desorption average pore diameter. def Determined by ICP-OES measurement. actual Ni,Ce content and Mg/Al.

3.2. Morphological Study and the Particle Size Analysis

The SEM images of the NiCe0-HT sample with the magnification of 10W and 5W were shown in **Figure 3a,c**, respectively. It was found that the NiCe0-HTexhibited platelet-like crystals that were aggregated as rosettes, referred to the typical characteristic for the hydrotalcite structure[42]. However, the morphology of the Ce-loading sample (NiCe5-HT) were found not changed apparently (**Figure 3b,d**). It further indicated that the hydrotalcite-like structure could be well generated, which was identical to the XRD results.

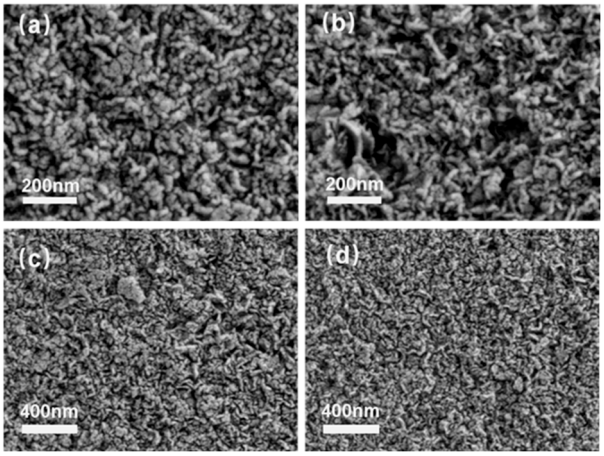

Figure 3. SEM images of (**a**) (**c**) NiCe0-HT, (**b**) (**d**) NiCe5-HT.

Preprints (www.preprints.org) | NOT PEER-REVIEWED | Posted: 23 May 2023 doi:10.20944/preprints202305.1552.v1

TEM measurements were used to observe the state of all the calcined and reduced NiCex-C catalysts. As shown in **Figure 4**, The dark spots were ascribed to the Ni nanoparticles dispersed on the frame of the mixed metal oxide. For all samples, the layered structure of the hydrotalcite precursors partially collapsed after calcination. The morphology and the Ni particle dispersion were varied due to the introduction of different Ce contents. For the Ce-containing catalysts, Ni nanoparticles dispersed evenly on the catalyst surface. While large clusters of Ni particles were observed on the surface of the NiCe0-C catalyst, the dispersion of Ni nanoparticles were poor. In addition, the well-defined lattice fringes assigned to the face-centered cubic Ni (111) surface were observed in HRTEM images for all samples, with an average lattice spacing of 0.2nm[4].

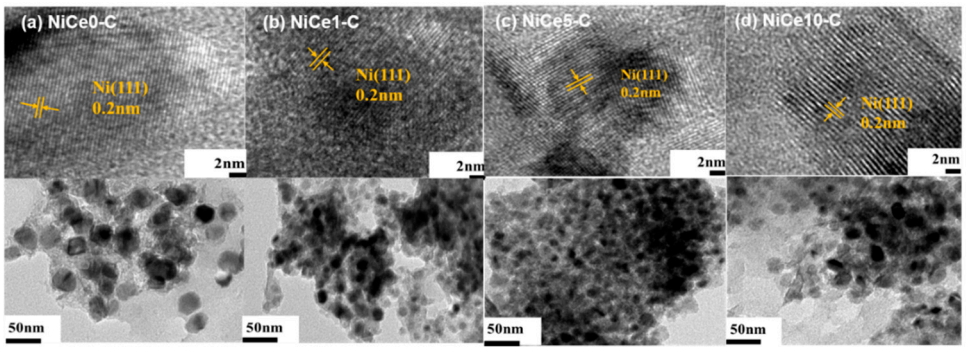

Figure 4. TEM and HRTEM images of the catalysts (**a**) NiCe0-C, (**b**) NiCe1-C, (**c**) NiCe5-C, (**d**) NiCe10-C.

Moreover, the frequency distribution histogram of Ni particle-size for all samples were displayed in **Figure 5**, ranged from 5nm-10nm. The small size of Ni nanoparticles probably due to the confinement effect of HT precursor[43], which processed the ordered metal oxides grids would confine the growth of the Ni particles and achieved the highly dispersed Ni particles [44,45]. Meanwhile, the corresponding average particle size was found to follow the order: NiCe5-C (5.67nm) < NiCe1-C (6.82nm) < NiCe10-C (7.71nm) < NiCe0-C (9.06nm). Optimal Ce element loading (5 wt%) led to the lowest Ni particle-size. In a word, the statistics and TEM images proved that the aggregation of Ni particle in the NiCe0-C catalyst could be halted to some extent by the incorporation of Ce element. Which would play a positive effect on the uniform dispersion of the Ni nanoparticles.

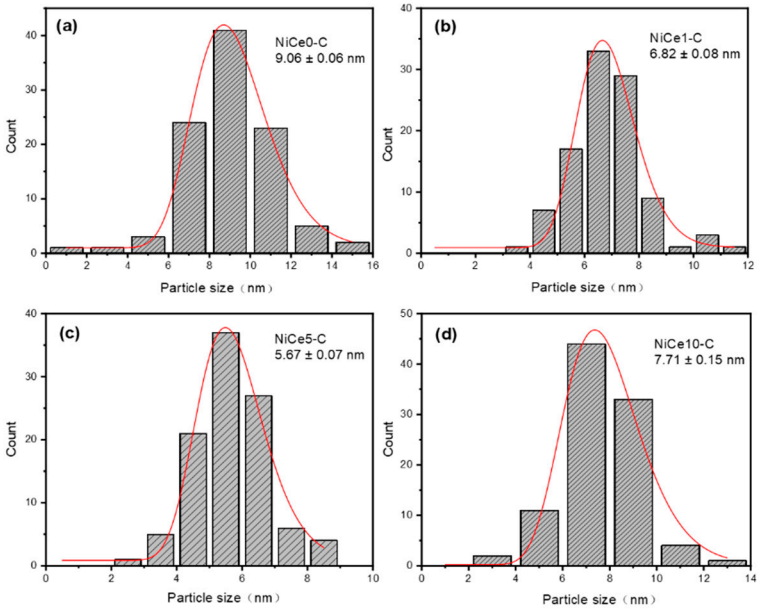

Figure 5. Metal particle-size distribution over the reduced by TEM images (**a**) NiCe0-C, (**b**) NiCe1-C, (**c**) NiCe5-C, (**d**) NiCe10-C.

Preprints (www.preprints.org) | NOT PEER-REVIEWED | Posted: 23 May 2023 doi:10.20944/preprints202305.1552.v1

3.3. Reducibility and Metal-Support Interaction Study

The reduction behavior of the NiCex-C (x=0,1,5,10) catalysts was evaluated by H_2-TPR analysis. H_2 consumption during the H_2-TPR experiments should be caused mainly by the reduction of NiO species. It was known that the reduction difficulty of NiO species might be determined by the metal-support interaction with the oxide support or the dispersion conditions over the support surface[37]. As shown in **Figure 6**, three types of the reduction peaks could be observed. The low-temperature reduction peak (~350℃) of NiO species can be ascribed to the weakly interacting with the support [46]. It could be found that the peak intensity (~350℃) gradually became weaker with the increasing of Ce contents. The peak temperature was decreased to 346℃ over NiCe1-C catalyst, compared to 360℃ for undoped NiCe0-C. This results indicated that after the addition of Ce element, this part of NiO was more easily reducible [47]. The minor shoulder peak (~510℃) was attributed to the reduction of a small amount of Ni^{2+} species, which are weakly bound to oxygen atoms at the Ni-O-Al (or Ce) interface, commonly reported in Ni/AlCeO-x catalysts[28]. Besides, for Ce-containing catalysts, this reduction peak also corresponded to the reduction of Ce^{4+} to Ce^{3+} species. [48]. The main reduction peak appeared at 700℃ for the NiCex-C catalysts, which was attributed to a stronger metal-support interaction between NiO species and the support matrix (Mg(Ce)AlO)[24]. To obtained sample with highly reduced, the reduction temperature in activity test was chosen to be about 700 ℃. Especially the reduction temperature of NiO in the NiCe5-C catalyst shifted to the lowest temperature of 690 ℃. Consequently, for these NiO species, the NiCe5-C catalyst displayed the best reduction behavior. However, when Ce element was incorporated into the catalyst, the high temperature peak (~700℃) became boarder with lower intensity. This result indicated that the strong metal-support interaction was weakened by the loading of Ce element[49]. Appropriate metal-support interaction would led to more Ni^0 active sites [50], thus giving preferable low temperature catalytic activity.

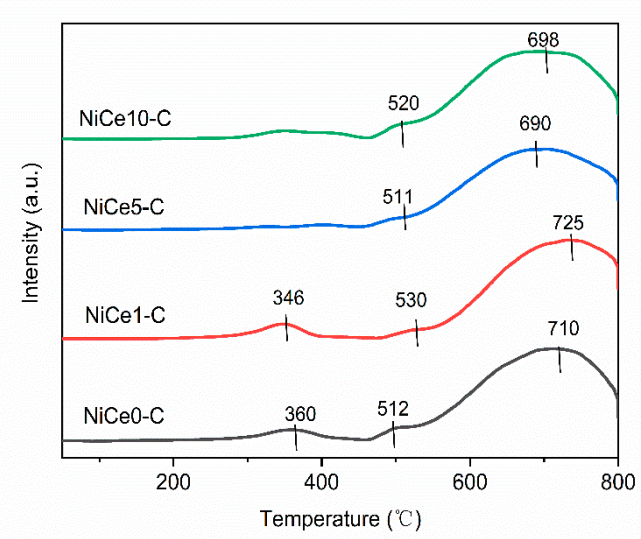

Figure 6. H_2-TPR profiles of NiCex-C (x=0,1,5,10) catalysts.

3.4. Surface Basicity and Element Distribution Analysis

In CO_2 methanation process, reaction molecule CO_2 was not directly absorbed on metal nickel, but on surface basic sites (OH^- groups or alkali/alkaline-earth metal oxides), which was beneficial to activate CO_2 [19,51,52]. Hence, CO_2-TPD was carried out for the NiCex-C catalysts to determine the basic strength and CO_2 adsorption capacity. As shown in **Figure 7**, the desorption curves of all the samples could be divided into three types of Gaussian peaks (α, β, γ peak). The three reduction peaks occurred at 100~120, 140~170, 250~280℃, respectively[7,11]. Which corresponding to weak-strength basic sites (α and β peak), medium-strength basic sites (γ peak). The weak-strength basic sites was attributed to the rapid formation of bicarbonate which was due to the weak adsorption of CO_2 by hydroxyl group on the catalyst surface[14]. While the medium basic sites were assigned to Lewis

Preprints (www.preprints.org) | NOT PEER-REVIEWED | Posted: 23 May 2023 doi:10.20944/preprints202305.1552.v1

basic sites (acid-base Ce^{4+}- O^{2-} and metal-O^{2-}pairs) associated with CO_2 adsorption. These basic sites bound CO_2 sufficiently strongly for its activation and subsequent reduction[53]. Based on the literature[54], the medium basic sites played an important role in CO_2 methanation process. From the previous report, the surface charge would be disturbed by introducing hetero-ions into the hydrotalcite layer[55]. Thus, the incorporation of Ce element into the nickel-based hydrotalcite obviously influenced the distribution of basic sites. Detailed information of surface basic sites relative content for all reduced NiCex-C samples was displayed in **Table 2.** The proportion of the medium basic sites were calculated and were found to follow the order: NiCe5-C > NiCe1-C> NiCe0-C> NiCe10-C. The quantities of CO_2 adsorbed on basic sites over reduced NiCex-C catalysts were summarized in **Table 3.** The highest density of medium-strength basic sites was found on the NiCe5-C sample (0.79mmol CO_2/g_{cat}), suggesting that CO_2 could be more easily activated, and further affected the catalytic performance. While the incorporation of 10wt.% of Ce element could lead to a slight decrease in total basicity (0.80mmol CO_2/g_{cat}). The NiCe10-C exhibited the lowest CO_2 adsorption capacity and thus the least amount of CO_2 for the methanation. The correlation between the surface basic sites and its catalytic activity in the CO_2 methanation will be further explored in ubsequent section [56].

Table 2. Fitting analysis and parameters of CO_2-TPD for all reduced NiCex-C samples.

Samples	Reduction temperature (℃)			Relative content (%)		
	α	β	γ	α	β	γ
NiCe0-C	108	173	277	16.1	36.2	47.7
NiCe1-C	100	145	250	13.9	35.5	50.6
NiCe5-C	117	170	264	11.9	30.3	57.8
NiCe10-C	103	154	245	14.3	40.5	45.2

Table 3. Surface basic sites density results of CO_2-TPD for all reduced NiCex-C samples.

Samples	Weak-strength basic sites (α+β) (mmol CO_2/g_{cat})	Medium-strength basic sites (γ) (mmol CO_2/g_{cat})	CO_2-adsorption amount (mmol CO_2/g_{cat})
NiCe0-C	0.48	0.43	0.91
NiCe1-C	0.59	0.61	1.20
NiCe5-C	0.58	0.79	1.37
NiCe10-C	0.44	0.36	0.80

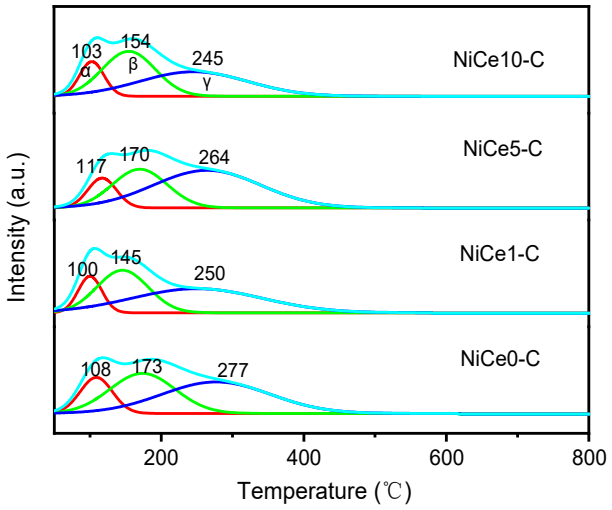

Figure 7. CO_2-TPD profiles of the NiCex-C catalysts.

Preprints (www.preprints.org) | NOT PEER-REVIEWED | Posted: 23 May 2023 doi:10.20944/preprints202305.1552.v1

The information of the surface components for the NiCex-C catalysts was further probed by XPS measurements. It was known that the position of the most intense peak was used to confirm the oxidation state of the metallic element and to obtain the information about the charge density for its cations[27]. As displayed in **Figure 8a,** the main band of the Ni $2p_{3/2}$ spectra for all the NiCex-C catalysts were deconvoluted into three peaks at ~ 853.8, ~856.6, and ~ 862.3 eV, corresponding to Ni^0, Ni^{2+} (bulk NiO), and satellite peak of nickel species[40]. From the literature, the satellite peak was assigned to Ni^{2+} species in Ni-O-Ce interaction interface or Ni^{2+} species in unreducible $NiAl_2O_4$ spinel [57]. These Ni species at higher binding energy (~856 and~ 862eV) suggested the strong metal-support interaction[58]. Based on the peak fitting and peak area calculation, the detailed information of Ni^0 species relative contents were listed in **Table 4**. Compared with the Ce-free sample, the Ni^0 relative content increased. In particular, the maximum value 40.5% for the NiCe5-C catalyst, while the minimum value 31.5% for the NiCe0-C catalyst. It was shown that the strong interaction between Ni^{2+} and support was weakened by the Ce dopants, leading to more Ni^0 species generated, which was consistent with the H_2-TPR results. Rare earth oxides might act as an electron donor so that more electrons were shifted to Ni species, resulting in an increase of d-electron density on the Ni surface. Similar to the reported (Sc, Y, Ce, and Pr) promoted NiMgAl catalysts for dry reforming of methane [59]. Meanwhile, this result also indicated that the introduction of Ce to the catalysts could promote the electron transfer and reduce more Ni^{2+} to Ni^0. While further increased the incorporation of Ce contents (10%), the proportion of Ni^0 shifted to the lower value (34.1%).

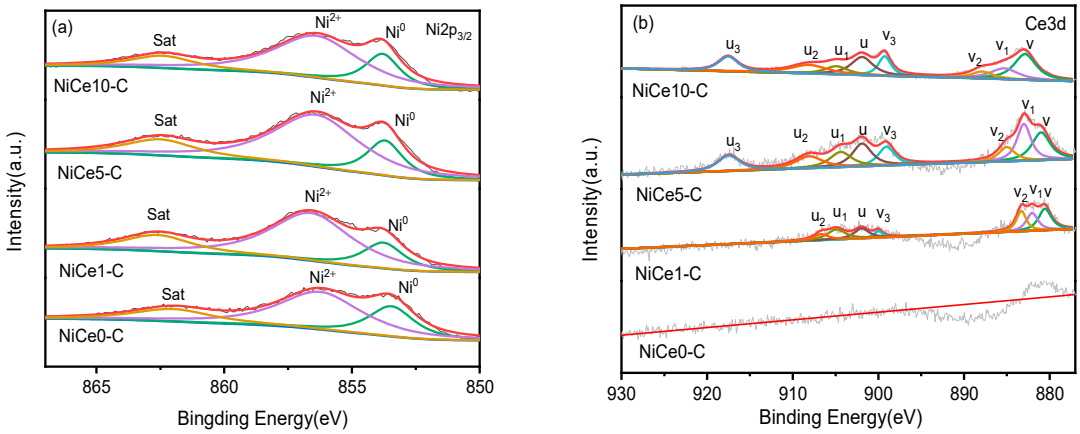

Figure 8. XPS spectrum of Ni $2p_{3/2}$ (**a**) and Ce3d (**b**) of the NiCex-C catalysts.

Table 4. XPS result of Ni^0 and Ce^{3+} relative content for the NiCex-C catalysts.

Samples	Relative content (%)	
	$Ni^0/(Ni^0+Ni^{2+})$	$Ce^{3+}/(Ce^{3+}+Ce^{4+})$
NiCe0-C	31.5	0.0
NiCe1-C	34.7	19.6
NiCe5-C	40.5	23.2
NiCe10-C	34.1	18.8

On the other hand, the two sets of Ce 3d spin–orbit coupling peaks, corresponding to 3d3/2 (labeled as u) and 3d5/2 (labeled as v) respectively, could be deconvoluted into eight peaks (**Figure 8b**). According to the literature, the oxidation states of cerium species mainly existed in the form of Ce^{3+} and Ce^{4+}[1]. More precisely, the peak near 882.8eV (v), 887.8eV (v_2), 899.2eV (v_3), 901.9eV (u), 908.1eV(u_2) 917.5eV(u_3) could be attributed to the Ce^{4+} species in CeO_2[46]. However, for the NiCe1-C catalyst with lower Ce-loading, the u_3 peak near 917.5eV was not noticeable from XPS spectra. Besides, the peak near 885.3eV(v_1) 904.9eV (u_1) could be ascribed to the Ce^{3+}state[60]. The Ce^{3+}state indicated the reduction of Ce^{4+} due to the high temperature hydrogen reduction[41]. In order to keep

charge balance of CeO_2, that oxygen vacancies were generated in this reduction process[46,61]. Thus the concentration of Ce^{3+} was in direct proportion to oxygen vacancies contents, which were the main active sites in CO_2 activation and absorption[8,62]. The concentrations of Ce^{3+} of all the NiCex-C catalysts were calculated by adding the areas under each deconvolution peak and dividing by the total peak area. The detailed molar ratio of Ce^{3+}/ (Ce^{3+} + Ce^{4+}) were tabulated in **Table 4**. It could be found the highest Ce^{3+} concentration of 23.2% for the NiCe5-C catalyst. Obviously higher than other Ce-containing catalysts. Demonstrating that there were more oxygen vacancies at the Ni–O-Ce interfaces. In a word, the NiCe5-C catalyst owed the most active sites for CO_2 absorption and activation as well as surface Ni^0 sites for the H_2 molecular splitting. They may work synergistically and efficiently in CO_2 hydrogenation under this reaction condition.

3.4. Catalytic Activity and Stability in CO_2 Methanation Reaction

The catalytic performance of all prepared NiCex-C (x=0, 1, 5, 10) catalysts for CO_2 methanation reaction were investigated at gas hourly space velocity (GHSV) of inlet gas of 15,000 mL/g_{cat}/h with H_2/CO_2 molar ratio of 4.0 in the temperature range of 200-350℃. It was known that CO_2 methanation process was exothermic so the total conversion could not be reached to 100% at high reaction temperature (＞200℃)[63]. CO_2 methanation performances of the NiCex-C catalysts were shown in **Figure 9**. As shown in **Figure 9a**, CO_2 conversion increased for all the samples with increasing reaction temperature. It was displayed a significant difference in performance at 250℃. CO_2 conversion increased at 250℃ from 11.7% for NiCe0-C to 30.2% and 80.0% for NiCe1-C and NiCe5-C, respectively. The maximum CO_2 conversion was observed at 300℃.Then the catalysts reached CO_2 equilibrium conversion above 300 ℃. T_{50} was used to identify the low-temperature activity of the samples[11]. The value of T_{50} was 263.8℃ and 258.4℃ for Ce-free NiCe0-C catalyst and NiCe1-C catalyst, respectively. While it was obviously decreased to 238.6℃ on NiCe5-C catalyst, indicating the promotion effect from Ce. However, when further increasing Ce content, the value of T_{50} increased to 277.9℃ for NiCe10-C catalyst. It could be found that the catalytic performance first increased and then decreased with the increase of Ce content. This excellent low-temperature performance of NiCe5-C was from two main aspects: (I) Abundant active Ni^0 sites evenly dispersed over the NiMgAl mixed metal oxide surface (XPS and TEM results), which provided active metal sites for H_2 molecular dissociation and further promoted the hydrogenation process[37]. (II) The medium basic sites were conducive to the CO_2 adsorption and activation[18]. NiCe5-C possessed a highest amounts of medium-strength basic sites (CO_2-TPD result). Nevertheless, NiCe10-C exhibited the worst hydrogenation activity. This could have been mainly caused by the lowest amounts of total basic sites, as confirmed by CO_2-TPD. Furthermore, CO as the main by-product in CO_2 methanation process was due to reverse water gas shift (RWGS) process: $CO_2 + H_2 = CO + H_2O$. It was a endothermic reaction favorable at high temperature[64]. The CH_4 Selectivity of NiCex-C catalysts presented high value nearly 100% (**Figure 9b**), and few CO by-product could be found at low reaction temperature. The detailed product distributions of the tested catalysts in the CO_2 methanation reaction at reaction temperature of 225℃ were displayed in **Table 5**. At 225℃, The CO_2 conversion of the Ce-free sample was only 3.4%, while that of NiCe5-C reached a maximum value of 13.9%. The CO_2 conversion rate (R_{CO2}) and the TOF (Turnover frequency) value of NiCe5-C were 4.1 times and 3 times higher than that of NiCe0-C, respectively. It indicated that the low-temperature activity of Ni-based catalyst derived from hydrotalcite-like precursors could be significantly enhanced by moderate Ce doped.

Preprints (www.preprints.org) | NOT PEER-REVIEWED | Posted: 23 May 2023 doi:10.20944/preprints202305.1552.v1

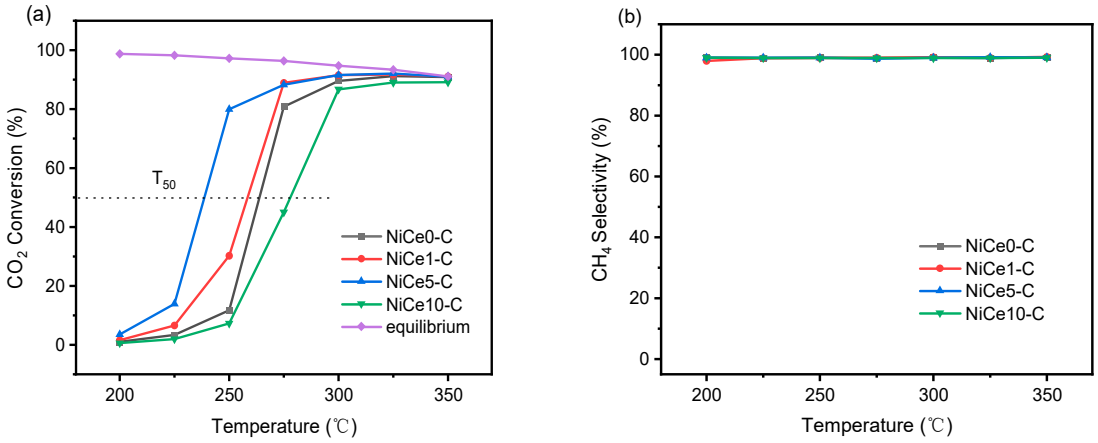

Figure 9. CO_2 conversion (**a**) and (**b**) CH_4 selectivity of NiCex-C catalysts with temperature range from 200-350℃, GHSV=15000 mL/g_{cat}/h H_2/CO_2=4 (molar ratio), 50 mL/min, 200 mg catalyst.

Table 5. Comparison of catalytic performance of NiCex-C (x= 0, 1, 5,10) catalysts in.CO_2 methanation at 225℃.

Samples	Conversion (%)	Selectivity (%)		RCO_2(μmolCO_2/g_{cat}/s)	TOF(h^{-1})
		CH_4	CO		
NiCe0-C	3.4	98.7	1.3	1.26	0.39
NiCe1-C	6.6	98.9	1.1	2.43	0.65
NiCe5-C	13.9	99.8	0.2	5.17	1.19
NiCe10-C	2.0	98.9	1.1	0.73	0.22
Reaction conditions:	T=225℃ (conversion < 15%), GHSV=15000 mL/g_{cat}/h H_2/CO_2=4 (molar ratio), 50 mL/min, 200 mg catalyst.				

The long-term stability of the catalyst was of great importance for industrial application. As shown in **Figure 10**, the stability of the NiCe5-C catalyst was investigated at 300 ℃ because of the best performance among all samples. After 80 h stability test, the NiCe5-C catalyst also exhibited high activity, with about 91.7% of CO_2 conversion and almost 100% of CH_4 selectivity. In addition, there was no obvious deviation for them under the 80h stability test. The NiCe5-C catalyst achieved high stability as well. It indicated that the well-dispersed nickel particles on the catalyst surface (TEM results) could enhance the anti-sintering ability of the NiCe5-C sample and avoid deactivation after long-term use.

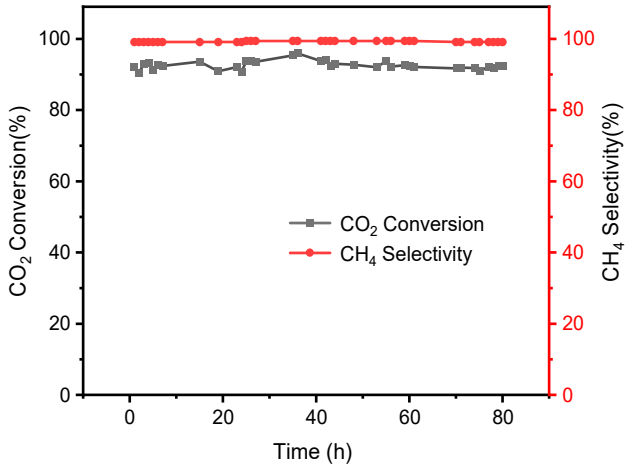

Figure 10. stability for CO_2 methanation over the NiCe5-C catalyst at 300℃. Reaction conditions: H_2/CO_2 = 4: 1, GHSV = 15000 mL/g_{cat}/h, 0.1Mpa.

Preprints (www.preprints.org) | NOT PEER-REVIEWED | Posted: 23 May 2023 doi:10.20944/preprints202305.1552.v1

Hydrogenation of CO_2 to methane was a first order reaction, and the reaction of H with CO_2 was the rate-controlling step for the this reaction[65]. The apparent activation energies of the samples were measured by the Arrhenius equation. As shown in **Figure 11**, take the logarithm of CO_2 conversion as x variable and the reciprocal of temperature as y variable to fit a straight line. The apparent activation energies of the catalysts were obtained by calculating the slop of the fitting lines. Compared to the NiCe0-C catalyst (98.13 kJ/mol), the apparent activation energy of the NiCe5-C catalyst was lower (96.04 kJ/mol). This result suggested the CO_2 methanation reaction was more facile on NiCe5-C catalyst. It could be attributed to the Ce element had a positive effect on promoting charge transfer from active metal to the CO_2 molecules[66]. Therefore, the reactant CO_2 molecules were more easily activated, which in favor of decreasing the energy barrier of H and CO_2 reaction.

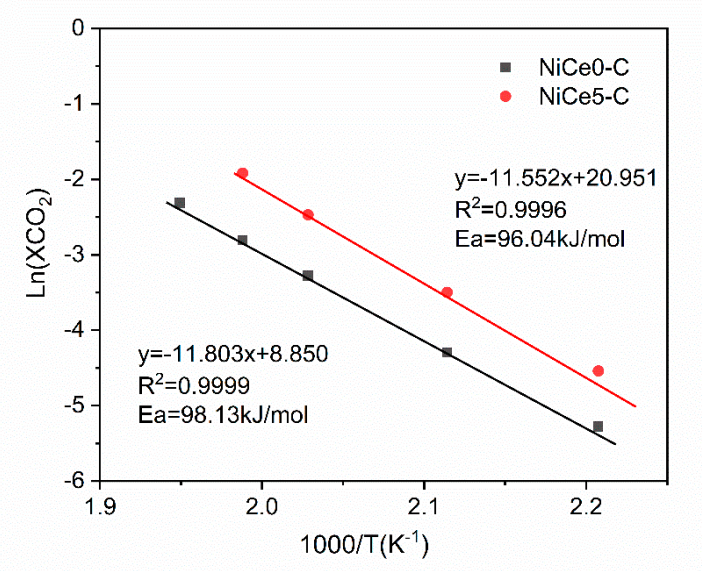

Figure 11. Arrehnius plots for the NiCe0-C and NiCe5-C catalysts.

3.5. The Descriptors of the Relationship between Catalytic Performance and Surface Basicity

On the basis of previous literature reports, the Lewis acid-base sites instead of strong basic site were involved in the CO_2 methanation mechanism[67,68]. Therefore, it was necessary to explore the relationship between catalytic activity and the number of medium basic sites. As plotted in **Figure 12a**, the highest CO_2 conversion at 225°C was achieved over the NiCe5-C with the strongest medium-strength basic sites. In addition, the CO_2 conversion of the catalysts was positively correlated with the number of medium basic sites. In this contribution, we observed the turnover frequency of the catalysts almost displayed linear relationship with the content of medium-strength basic sites at 225°C (**Figure 12b**). It showed that the TOF values increased with increasing amount of medium-strength basic sites. These results demonstrate that the variation of Ce content could effectively regulate the number of medium-strength basic sites on the surface of NiCex-C, and the medium-strength basic sites on the catalyst played a crucial role in achieving high catalytic activity for CO_2 methanation at low temperatures.

Preprints (www.preprints.org) | NOT PEER-REVIEWED | Posted: 23 May 2023 doi:10.20944/preprints202305.1552.v1

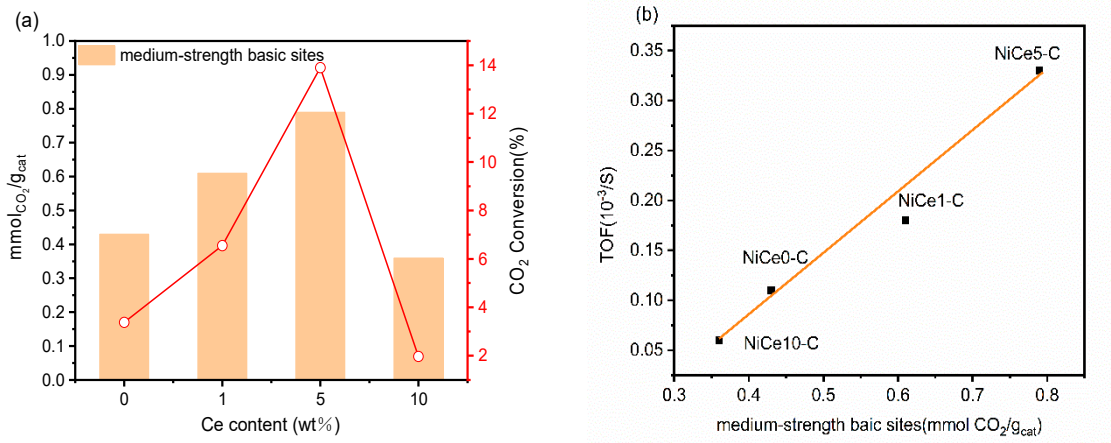

Figure 12. (**a**) Effect of Ce content on the medium-strength basic sites and CO_2 conversion (T=225°C) (**b**) The relationship between medium-strength basic sites and TOF (T=225°C).

4. Conclusions

In this work, we demonstrated an extremely straightforward method of preparing Ce-promoted NiMgAl hydrotalcite-derived catalysts via co-precipitation operation, to promote CO_2 methanation at low temperatures. The NiCe5-C sample exhibited superior low-temperature activity for CO_2 methanation (CO_2 conversion: 80.0%, CH_4 selectivity >99%, GHSV=15,000mL/gcat/h, H_2/CO_2 =4, 250°C, 0.1Mpa), together with high stability. While the CO_2 conversion of the Ce-free sample was only 11.7% under the same conditions. At 225°C, TOF value of the NiCe5-C (1.19 h^{-1}) was three times higher than that of NiCe0-C (0.39 h^{-1}). The characterization results indicated that incorporation of appropriate amount of Ce into NiMgAl could weaken the strong metal- support interaction, thereby promoting the reduction of NiO species. Meanwhile, the Ce element could efficiently regulate the surface basic species. The medium-basic sites were found to have a good linear correlation with TOF. The NiCe5-C catalyst owed the highest ratio of $Ni^0/(Ni^{2+}+Ni^0)$ and rich medium-basic sites, was able to work more effectively on dissociating H_2 and activating CO_2, and further hydrogenated to methane. Our contribution provided a promising and practical thought to raise the catalytic performance in the CO_2 methanation at low-temperature.

References

1. Bian, Y.; Xu, C.; Wen, X.; Xu, L.; Cui, Y.; Wang, S.; Wu, C.-e.; Qiu, J.; Cheng, G.; Chen, M., CO_2 methanation over the Ni-based catalysts supported on nano-CeO_2 with varied morphologies. *Fuel* **2023,** 331.
2. Tada, S.; Kikuchi, R., Mechanistic study and catalyst development for selective carbon monoxide methanation. *Catalysis Science & Technology* **2015,** 5, (6), 3061-3070.
3. Lin, J.; Ma, C.; Wang, Q.; Xu, Y.; Ma, G.; Wang, J.; Wang, H.; Dong, C.; Zhang, C.; Ding, M., Enhanced low-temperature performance of CO_2 methanation over mesoporous Ni/Al_2O_3-ZrO_2 catalysts. *Applied Catalysis B: Environmental* **2019,** 243, 262-272.
4. Varvoutis, G.; Lykaki, M.; Stefa, S.; Binas, V.; Marnellos, G. E.; Konsolakis, M., Deciphering the role of Ni particle size and nickel-ceria interfacial perimeter in the low-temperature CO_2 methanation reaction over remarkably active Ni/CeO_2 nanorods. *Applied Catalysis B: Environmental* **2021,** 297.
5. Kopyscinski, J.; Schildhauer, T. J.; Biollaz, S. M. A., Production of synthetic natural gas (SNG) from coal and dry biomass – A technology review from 1950 to 2009. *Fuel* **2010,** 89, (8), 1763-1783.
6. Zhen, W.; Gao, F.; Tian, B.; Ding, P.; Deng, Y.; Li, Z.; Gao, H.; Lu, G., Enhancing activity for carbon dioxide methanation by encapsulating (1 1 1) facet Ni particle in metal–organic frameworks at low temperature. *Journal of Catalysis* **2017,** 348, 200-211.
7. Summa, P.; Swirk, K.; Wierzbicki, D.; Motak, M.; Alxneit, I.; Ronning, M.; Da Costa, P., Co-Precipitated Ni-Mg-Al Hydrotalcite-Derived Catalyst Promoted with Vanadium for CO_2 Methanation. *Molecules* **2021,** 26, (21).
8. Rui, N.; Zhang, X.; Zhang, F.; Liu, Z.; Cao, X.; Xie, Z.; Zou, R.; Senanayake, S. D.; Yang, Y.; Rodriguez, J. A.; Liu, C.-J., Highly active Ni/CeO_2 catalyst for CO_2 methanation: Preparation and characterization. *Applied Catalysis B: Environmental* **2021,** 282.

9. Aziz, M. A. A.; Jalil, A. A.; Triwahyono, S.; Ahmad, A., CO_2 methanation over heterogeneous catalysts: recent progress and future prospects. *Green Chemistry* **2015,** 17, (5), 2647-2663.
10. Mutz, B.; Carvalho, H. W. P.; Mangold, S.; Kleist, W.; Grunwaldt, J.-D., Methanation of CO_2: Structural response of a Ni-based catalyst under fluctuating reaction conditions unraveled by operando spectroscopy. *Journal of Catalysis* **2015,** 327, 48-53.
11. Xiao, X.; Wang, J.; Li, J.; Dai, H.; Jing, F.; Liu, Y.; Chu, W., Enhanced low-temperature catalytic performance in CO_2 hydrogenation over Mn-promoted NiMgAl catalysts derived from quaternary hydrotalcite-like compounds. *International Journal of Hydrogen Energy* **2021,** 46, (66), 33107-33119.
12. Ma, L.; Ye, R.; Huang, Y.; Reina, T. R.; Wang, X.; Li, C.; Zhang, X. L.; Fan, M.; Zhang, R.; Liu, J., Enhanced low-temperature CO_2 methanation performance of Ni/ZrO_2 catalysts via a phase engineering strategy. *Chemical Engineering Journal* **2022,** 446.
13. Yan, Y.; Dai, Y.; He, H.; Yu, Y.; Yang, Y., A novel W-doped Ni-Mg mixed oxide catalyst for CO_2 methanation. *Applied Catalysis B: Environmental* **2016,** 196, 108-116.
14. He, F.; Zhuang, J.; Lu, B.; Liu, X.; Zhang, J.; Gu, F.; Zhu, M.; Xu, J.; Zhong, Z.; Xu, G.; Su, F., Ni-based catalysts derived from Ni-Zr-Al ternary hydrotalcites show outstanding catalytic properties for low-temperature CO_2 methanation. *Applied Catalysis B: Environmental* **2021,** 293.
15. Dębek, R.; Radlik, M.; Motak, M.; Galvez, M. E.; Turek, W.; Da Costa, P.; Grzybek, T., Ni-containing Ce-promoted hydrotalcite derived materials as catalysts for methane reforming with carbon dioxide at low temperature – On the effect of basicity. *Catalysis Today* **2015,** 257, 59-65.
16. Li, C.; Wei, M.; Evans, D. G.; Duan, X., Layered double hydroxide-based nanomaterials as highly efficient catalysts and adsorbents. *Small* **2014,** 10, (22), 4469-86.
17. Liu, J.; Bing, W.; Xue, X.; Wang, F.; Wang, B.; He, S.; Zhang, Y.; Wei, M., Alkaline-assisted Ni nanocatalysts with largely enhanced low-temperature activity toward CO_2 methanation. *Catalysis Science & Technology* **2016,** 6, (11), 3976-3983.
18. Guo, X.; Gao, D.; He, H.; Traitangwong, A.; Gong, M.; Meeyoo, V.; Peng, Z.; Li, C., Promotion of CO_2 methanation at low temperature over hydrotalcite-derived catalysts-effect of the tunable metal species and basicity. *International Journal of Hydrogen Energy* **2021,** 46, (1), 518-530.
19. Wang, J.; Xiao, X.; Li, J.; Gao, X.; Zheng, J.; Chu, W., Hydrotalcite-derived Ni-LDO catalysts via new approach for enhanced performances in CO_2 catalytic reduction. *Fuel* **2022,** 324, (2022), 124491.
20. Wang Y, X. Y., Liu Q, Sun J, Ji S, Z.j. Wang., Enhanced low-temperature activity for CO2 methanation over NiMgAl_SiC. *J Chem Technol Biotechnol* **2019,** 94, 3780–6.
21. Du, X.; Zhang, D.; Gao, R.; Huang, L.; Shi, L.; Zhang, J., Design of modular catalysts derived from NiMgAl-LDH@m-SiO_2 with dual confinement effects for dry reforming of methane. *Chem Commun (Camb)* **2013,** 49, (60), 6770-2.
22. Wierzbicki, D.; Debek, R.; Motak, M.; Grzybek, T.; Gálvez, M. E.; Da Costa, P., Novel Ni-La-hydrotalcite derived catalysts for CO_2 methanation. *Catalysis Communications* **2016,** 83, 5-8.
23. Sun, C.; Świrk, K.; Wierzbicki, D.; Motak, M.; Grzybek, T.; Da Costa, P., On the effect of yttrium promotion on Ni-layered double hydroxides-derived catalysts for hydrogenation of CO_2 to methane. *International Journal of Hydrogen Energy* **2021,** 46, (22), 12169-12179.
24. Taufiq-Yap, Y. H.; Sudarno; Rashid, U.; Zainal, Z., CeO_2–SiO_2 supported nickel catalysts for dry reforming of methane toward syngas production. *Applied Catalysis A: General* **2013,** 468, 359-369.
25. Montini, T.; Melchionna, M.; Monai, M.; Fornasiero, P., Fundamentals and Catalytic Applications of CeO_2-Based Materials. *Chem Rev* **2016,** 116, (10), 5987-6041.
26. Dębek, R.; Motak, M.; Galvez, M. E.; Grzybek, T.; Da Costa, P., Influence of Ce/Zr molar ratio on catalytic performance of hydrotalcite-derived catalysts at low temperature CO_2 methane reforming. *International Journal of Hydrogen Energy* **2017,** 42, (37), 23556-23567.
27. Cárdenas-Arenas, A.; Quindimil, A.; Davó-Quiñonero, A.; Bailón-García, E.; Lozano-Castelló, D.; De-La-Torre, U.; Pereda-Ayo, B.; González-Marcos, J. A.; González-Velasco, J. R.; Bueno-López, A., Isotopic and in situ DRIFTS study of the CO_2 methanation mechanism using Ni/CeO_2 and Ni/Al_2O_3 catalysts. *Applied Catalysis B: Environmental* **2020,** 265.
28. Zhang, J.; Ren, B.; Fan, G.; Yang, L.; Li, F., Exceptional low-temperature activity of a perovskite-type $AlCeO_3$ solid solution-supported Ni-based nanocatalyst towards CO_2 methanation. *Catalysis Science & Technology* **2021,** 11, (11), 3894-3904.
29. Dębek, R.; Galvez, M. E.; Launay, F.; Motak, M.; Grzybek, T.; Da Costa, P., Low temperature dry methane reforming over Ce, Zr and CeZr promoted Ni–Mg–Al hydrotalcite-derived catalysts. *International Journal of Hydrogen Energy* **2016,** 41, (27), 11616-11623.
30. Wierzbicki, D.; Baran, R.; Dębek, R.; Motak, M.; Grzybek, T.; Gálvez, M. E.; Da Costa, P., The influence of nickel content on the performance of hydrotalcite-derived catalysts in CO_2 methanation reaction. *International Journal of Hydrogen Energy* **2017,** 42, (37), 23548-23555.

31. Lin, S.; Hao, Z.; Shen, J.; Chang, X.; Huang, S.; Li, M.; Ma, X., Enhancing the CO_2 methanation activity of Ni/CeO_2 via activation treatment-determined metal-support interaction. *Journal of Energy Chemistry* **2021,** 59, 334-342.
32. Guo, X.; Peng, Z.; Hu, M.; Zuo, C.; Traitangwong, A.; Meeyoo, V.; Li, C.; Zhang, S., Highly Active Ni-Based Catalyst Derived from Double Hydroxides Precursor for Low Temperature CO_2 Methanation. *Industrial & Engineering Chemistry Research* **2018,** 57, (28), 9102-9111.
33. Gao, J.; Jiang, Q.; Liu, Y.; Liu, W.; Chu, W.; Su, D. S., Probing the enhanced catalytic activity of carbon nanotube supported Ni-LaO(x) hybrids for the CO(2) reduction reaction. *Nanoscale* **2018,** 10, (29), 14207-14219.
34. Wang, X.; Liu, Q.; Jiang, J.; Jin, G.; Li, H.; Gu, F.; Xu, G.; Zhong, Z.; Su, F., SiO2-stabilized Ni/t-ZrO_2 catalysts with ordered mesopores: one-pot synthesis and their superior catalytic performance in CO methanation. *Catalysis Science & Technology* **2016,** 6, (10), 3529-3543.
35. Xu, X.; Liu, L.; Tong, Y.; Fang, X.; Xu, J.; Jiang, D.-e.; Wang, X., Facile Cr^{3+}-Doping Strategy Dramatically Promoting Ru/CeO_2 for Low-Temperature CO_2 Methanation: Unraveling the Roles of Surface Oxygen Vacancies and Hydroxyl Groups. *ACS Catalysis* **2021,** 11, (9), 5762-5775.
36. Asencios, Y. J. O.; Elias, K. F. M.; Assaf, E. M., Oxidative-reforming of model biogas over NiO/Al_2O_3 catalysts: The influence of the variation of support synthesis conditions. *Applied Surface Science* **2014,** 317, 350-359.
37. Zhang, Q.; Xu, R.; Liu, N.; Dai, C.; Yu, G.; Wang, N.; Chen, B., In situ Ce-doped catalyst derived from NiCeAl-LDHs with enhanced low-temperature performance for CO_2 methanation. *Applied Surface Science* **2022,** 579.
38. Tanasoi, S.; Mitran, G.; Tanchoux, N.; Cacciaguerra, T.; Fajula, F.; Săndulescu, I.; Tichit, D.; Marcu, I.-C., Transition metal-containing mixed oxides catalysts derived from LDH precursors for short-chain hydrocarbons oxidation. *Applied Catalysis A: General* **2011,** 395, (1-2), 78-86.
39. Tao, M.; Meng, X.; Lv, Y.; Bian, Z.; Xin, Z., Effect of impregnation solvent on Ni dispersion and catalytic properties of Ni/SBA-15 for CO methanation reaction. *Fuel* **2016,** 165, 289-297.
40. Kim, M.-J.; Youn, J.-R.; Kim, H. J.; Seo, M. W.; Lee, D.; Go, K. S.; Lee, K. B.; Jeon, S. G., Effect of surface properties controlled by Ce addition on CO_2 methanation over Ni/Ce/Al_2O_3 catalyst. *International Journal of Hydrogen Energy* **2020,** 45, (46), 24595-24603.
41. Guo, X.; He, H.; Traitangwong, A.; Gong, M.; Meeyoo, V.; Li, P.; Li, C.; Peng, Z.; Zhang, S., Ceria imparts superior low temperature activity to nickel catalysts for CO_2 methanation. *Catalysis Science & Technology* **2019,** 9, (20), 5636-5650.
42. Bette, N.; Thielemann, J.; Schreiner, M.; Mertens, F., Methanation of CO_2 over a (Mg,Al)OxSupported Nickel Catalyst Derived from a (Ni,Mg,Al)-Hydrotalcite-like Precursor. *ChemCatChem* **2016,** 8, (18), 2903-2906.
43. Du, X.; Zhang, D.; Shi, L.; Gao, R.; Zhang, J., Coke- and sintering-resistant monolithic catalysts derived from in situ supported hydrotalcite-like films on Al wires for dry reforming of methane. *Nanoscale* **2013,** 5, (7), 2659-63.
44. Xiao, X.; Gao, J.; Xi, S.; Lim, S. H.; Png, A. K. W.; Borgna, A.; Chu, W.; Liu, Y., Experimental and in situ DRIFTs studies on confined metallic copper stabilized Pd species for enhanced CO_2 reduction to formate. *Applied Catalysis B: Environmental* **2022,** 309.
45. Duarte, R. B.; Nachtegaal, M.; Bueno, J. M. C.; van Bokhoven, J. A., Understanding the effect of Sm_2O_3 and CeO_2 promoters on the structure and activity of Rh/Al_2O_3 catalysts in methane steam reforming. *Journal of Catalysis* **2012,** 296, 86-98.
46. Du, Y.; Qin, C.; Xu, Y.; Xu, D.; Bai, J.; Ma, G.; Ding, M., Ni nanoparticles dispersed on oxygen vacancies-rich CeO_2 nanoplates for enhanced low-temperature CO_2 methanation performance. *Chemical Engineering Journal* **2021,** 418.
47. Sato, A. G.; Volanti, D. P.; Meira, D. M.; Damyanova, S.; Longo, E.; Bueno, J. M. C., Effect of the ZrO_2 phase on the structure and behavior of supported Cu catalysts for ethanol conversion. *Journal of Catalysis* **2013,** 307, 1-17.
48. Amin, R.; Chang, X.; Liu, B., Synergistic Effect of CeO_2 in CH_4/CO_2 Dry Reforming Reaction over Stable xCeO_2 yNi/MCM-22 Catalysts. *Industrial & Engineering Chemistry Research* **2017,** 56, (26), 7445-7453.
49. Wu, Y.; Lin, J.; Ma, G.; Xu, Y.; Zhang, J.; Samart, C.; Ding, M., Ni nanocatalysts supported on mesoporous Al_2O_3-CeO_2 for CO_2 methanation at low temperature. *RSC Adv* **2020,** 10, (4), 2067-2072.
50. Li, W.; Liu, Y.; Mu, M.; Ding, F.; Liu, Z.; Guo, X.; Song, C., Organic acid-assisted preparation of highly dispersed Co/ZrO_2 catalysts with superior activity for CO_2 methanation. *Applied Catalysis B: Environmental* **2019,** 254, 531-540.
51. Satthawong, R.; Koizumi, N.; Song, C.; Prasassarakich, P., Bimetallic Fe–Co catalysts for CO_2 hydrogenation to higher hydrocarbons. *Journal of CO_2 Utilization* **2013,** 3-4, 102-106.

52. Li, Y.; Men, Y.; Liu, S.; Wang, J.; Wang, K.; Tang, Y.; An, W.; Pan, X.; Li, L., Remarkably efficient and stable Ni/Y_2O_3 catalysts for CO_2 methanation: Effect of citric acid addition. *Applied Catalysis B: Environmental* **2021,** 293.
53. Liu, Z.; Gao, X.; Liu, B.; Song, W.; Ma, Q.; Zhao, T.-s.; Wang, X.; Bae, J. W.; Zhang, X.; Zhang, J., Highly stable and selective layered Co-Al-O catalysts for low-temperature CO_2 methanation. *Applied Catalysis B: Environmental* **2022,** 310.
54. Dai, Y.; Xu, M.; Wang, Q.; Huang, R.; Jin, Y.; Bian, B.; Tumurbaatar, C.; Ishtsog, B.; Bold, T.; Yang, Y., Enhanced activity and stability of Ni/$La_2O_2CO_3$ catalyst for CO_2 methanation by metal-carbonate interaction. *Applied Catalysis B: Environmental* **2020,** 277.
55. Wierzbicki, D.; Baran, R.; Dębek, R.; Motak, M.; Gálvez, M. E.; Grzybek, T.; Da Costa, P.; Glatzel, P., Examination of the influence of La promotion on Ni state in hydrotalcite-derived catalysts under CO_2 methanation reaction conditions: Operando X-ray absorption and emission spectroscopy investigation. *Applied Catalysis B: Environmental* **2018,** 232, 409-419.
56. Xu, Y.; Wu, Y.; Li, J.; Wei, S.; Gao, X.; Wang, P., Combustion-impregnation preparation of Ni/SiO_2 catalyst with improved low-temperature activity for CO_2 methanation. *International Journal of Hydrogen Energy* **2021,** 46, (40), 20919-20929.
57. Weidler, N.; Schuch, J.; Knaus, F.; Stenner, P.; Hoch, S.; Maljusch, A.; Schäfer, R.; Kaiser, B.; Jaegermann, W., X-ray Photoelectron Spectroscopic Investigation of Plasma-Enhanced Chemical Vapor Deposited NiOx, NiOx(OH)y, and CoNiOx(OH)y: Influence of the Chemical Composition on the Catalytic Activity for the Oxygen Evolution Reaction. *The Journal of Physical Chemistry C* **2017,** 121, (12), 6455-6463.
58. Wu, H.; Pantaleo, G.; La Parola, V.; Venezia, A. M.; Collard, X.; Aprile, C.; Liotta, L. F., Bi- and trimetallic Ni catalysts over Al2O_3 and Al_2O_3-MO (M = Ce or Mg) oxides for methane dry reforming: Au and Pt additive effects. *Applied Catalysis B: Environmental* **2014,** 156-157, 350-361.
59. Cao, Y.; Li, H.; Zhang, J.; Shi, L.; Zhang, D., Promotional effects of rare earth elements (Sc, Y, Ce, and Pr) on NiMgAl catalysts for dry reforming of methane. *RSC Advances* **2016,** 6, (113), 112215-112225.
60. Ang, M. L.; Oemar, U.; Kathiraser, Y.; Saw, E. T.; Lew, C. H. K.; Du, Y.; Borgna, A.; Kawi, S., High-temperature water–gas shift reaction over Ni/xK/CeO_2 catalysts: Suppression of methanation via formation of bridging carbonyls. *Journal of Catalysis* **2015,** 329, 130-143.
61. Lin, B.; Lei, Z.; Xu, F.; Cheng, N.; Mu, S., Poly(vinylpyrrolidone) tailored porous ceria as a carbon-free support for methanol electrooxidation. *Electrochimica Acta* **2018,** 290, 55-62.
62. Li, W.; Nie, X.; Jiang, X.; Zhang, A.; Ding, F.; Liu, M.; Liu, Z.; Guo, X.; Song, C., ZrO2 support imparts superior activity and stability of Co catalysts for CO_2 methanation. *Applied Catalysis B: Environmental* **2018,** 220, 397-408.
63. Gao, J.; Jiang, Q.; Liu, Y.; Liu, W.; Chu, W.; Su, D. S., Probing the enhanced catalytic activity of carbon nanotube supported Ni-LaOx hybrids for the CO_2 reduction reaction. *Nanoscale* **2018,** 10, (29), 14207-14219.
64. Gao, J.; Wang, Y.; Ping, Y.; Hu, D.; Xu, G.; Gu, F.; Su, F., A thermodynamic analysis of methanation reactions of carbon oxides for the production of synthetic natural gas. *RSC Advances* **2012,** 2, (6).
65. Cai, M.; Wen, J.; Chu, W.; Cheng, X.; Li, Z., Methanation of carbon dioxide on Ni/ZrO_2-Al_2O_3 catalysts: Effects of ZrO_2 promoter and preparation method of novel ZrO_2-Al_2O_3 carrier. *Journal of Natural Gas Chemistry* **2011,** 20, (3), 318-324.
66. Wang, W.; Chu, W.; Wang, N.; Yang, W.; Jiang, C., Mesoporous nickel catalyst supported on multi-walled carbon nanotubes for carbon dioxide methanation. *International Journal of Hydrogen Energy* **2016,** 41, (2), 967-975.
67. Pan, Q.; Peng, J.; Sun, T.; Wang, S.; Wang, S., Insight into the reaction route of CO_2 methanation: Promotion effect of medium basic sites. *Catalysis Communications* **2014,** 45, 74-78.
68. Zhang, L.; Bian, L.; Zhu, Z.; Li, Z., La-promoted Ni/Mg-Al catalysts with highly enhanced low-temperature CO_2 methanation performance. *International Journal of Hydrogen Energy* **2018,** 43, (4), 2197-2206.